Article
Vol. 23, No. 6, p. 961–975, December 2019
https://doi.org/10.1007/s12303-019-0005-z
pISSN 1226-4806 eISSN 1598-7477
Geosciences Journal GJ

# Effect of pre-existing faults on the distribution of lower crust exhumation under extension: numerical modelling and implications for NW Ghana

Xiaojun Feng[1,2]*, Enyuan Wang[1], Prince O. Amponsah[3], Jérôme Ganne[2], Roland Martin[2], and Mark W. Jessell[2,4]

[1]School of Safety Engineering, China University of Mining and Technology, Xuzhou 221116, China
[2]Geosciences Environnement Toulouse, Observatoire Midi Pyrénées, Toulouse 31400, France
[3]School of Physical and Mathematical Sciences, Department of Earth Science, University of Ghana, P.O. Box LG 58, Legon-Accra, Ghana
[4]Centre for Exploration Targeting, The University of Western Australia, Perth, WA 6009, Australia

**ABSTRACT:** 3D thermo-mechanical models have been constructed to explore the influence of pre-existing faults on the temporal-spatial distribution of high-grade amphibolite-granulite facies metamorphic rocks during extension. The different dip amounts of three pre-existing faults (refer to the Bole-Nangodi shear zones, the Jirapa shear zone and the Bulenga shear zone in the study area) are studied in models. The results show the lower crust exhumes occur at a relatively low rate prior to attaining a Stretching Factor = 4.2%. The partially molten lower crustal rocks tend to move (up to 20 km) towards the center of the model and focus exhumation in regions where pre-existing faults intersect. The high-strain corridors in models are used to understand the loci of exhumation in the Bole-Bulenga domain of NW Ghana. Accordingly, in the eastern and western parts of the high-grade rock corridors in NW Ghana, partially molten rocks exhumed from the lower into middle-upper crustal levels are interpreted to have been dominantly facilitated by the km-scale high-strain corridors. In the central part of the Bole-Bulenga domain, the high-grade rocks are interpreted to have been exhumed because of a coupling between two mechanisms: (1) The exhumation of partially molten rocks between the Jirapa and Bole-Nangodi faults increases in spatially due to the reduction in space from north to south. (2) The exhumation of lower partially molten rocks in the central part, as a result of inherited orthogonal (E-W) structures.

**Key words:** metamorphic rocks, numerical modeling, exhumation, Eburnean Orogeny, strike-slip faults

Manuscript received November 15, 2018; Manuscript accepted February 22, 2019

## 1. INTRODUCTION

Pre-existing discontinuities in the crust generally provide sites for strain concentration (Jessell and Lister, 1991; Morley et al., 2004; Bellahsen and Daniel, 2005; Willingshofer et al., 2005; Misra and Mukherjee, 2015). The role of the orientation of such discontinuities on growth and re-activation of fault systems has been widely explored in numerical (D'Agostino et al., 1998; Feng et al., 2016b) and analogue (Imber et al., 2004; Dooley et al., 2012) models, as well as field investigations (Thatcher and Hill, 1991; Hand and Sandiford, 1999; Mukherjee et al., 2017).

The formation of metamorphic core complexes (MCCs) is generally related to extensional and strike-slip (e.g., Coney, 1980; Mukherjee, 2013; Denèle et al., 2017; Feng et al., 2018a) tectonics. This is characterized by the exhumation of partially molten lower crustal materials (Mukherjee, 2011, 2012, 2013; Mukherjee and Mulchrone, 2012, 2013) up to the upper crustal levels (Lister and Davis, 1989). Although numerous 2D-numerical (Burg et al., 2009; Choi et al., 2013) and analogue (Brun et al., 1994; Tirel et al., 2006; Sokoutis et al., 2007) models have been used to study the formation processes of MCCs in extensional tectonic settings, the use of 3D numerical modelling (Le Pourhiet et al., 2012; Rey et al., 2017) including pre-existing faults remains largely unexplored.

*Corresponding author:
Xiaojun Feng
School of Safety Engineering, China University of Mining and Technology, Xuzhou 221116, China
Tel: +86-0516-8388-4695, E-mail: xiaojun.feng@cumt.edu.cn

**Electronic supplementary material**
The online version of this article (https://doi.org/10.1007/s12303-019-0005-z) contains supplementary material, which is available to authorized users.

The emplacement of partially molten rocks into the upper crust can be assisted by pre-existing and new-formed faults (Neves et al., 1996; Vigneresse and Tikoff, 1999). In the high-grade Bole-Bulenga Terrane (BBT) of NW Ghana, three high-strain zones separate high-grade rocks (amphibolite-migmatite facies) from adjacent low-grade greenstone belts (Block et al., 2015, 2016; Feng, 2016; Feng et al., 2016a). These high-strain zones are known as the Bole-Nangodi shear zones, the Jirapa shear zone and the Bulenga shear zone (Fig. 1). The BBT was mainly deformed by two phases (D1 and D2). According to Block et al. (2015) and Block (2015), the EW Bulenga shear zone (about 80 km length) is a consequence of the D1 phase. The preliminary form of the NE-SW Bole-Nangodi shear (about 300 km length) zones resulted from the processes of bringing low- and high-grade rocks in contact during the D1 phase. Some inherited structures of the NS Jirapa shear zone (about 200 km length) also appeared in this stage. During the D2 N-S extension stage, there faults were reactivated in extension (West, 1993), a large amount of amphibolite-migmatites exhumed along these fault zones between 2137 ± 8 Ma and 2127 ± 7 Ma (Block et al., 2015).

In order to understand how pre-existing faults contribute and influence the exhumation processes under extension, ten 3D models (with differently oriented faults) related to the high-grade BBT geometry have been constructed. The models were constrained by the metamorphic rock record observed by Block et al. (2015). This study may shed light on the effect of orientation of pre-existing faults on the formation and development processes of lower crust exhumation during extension.

## 2. GEOLOGY

### 2.1. The West African Craton (WAC)

The WAC consists of three major Archaean and Paleoproterozoic blocks (Fig. 1a) namely, the Réguibat Shield to the north, the Leo-Man shield to the south and the smaller central Kenieba and Kayes Inliers (Jessell et al., 2016). The Leo-Man shield in the south is characterized by sequences of volcano-sedimentary and plutonic belts designated as parallel bands on a crustal scale. This parallel band architecture is not observed in the Réguibat Shield, suggesting probably a different geodynamic setting of formation. The western halves of both the Reguibat and the Leo-Man shield are marked by Archean rocks and the eastern halves by Paleoproterozoic rocks. The Paleoproterozoic block of the Leo-Man shield (also known as the Birimian domain or Baoule-Mossi domain) is marked by a geodynamic setting suggestive of immature volcanic arc (Dioh et al., 2006) or an oceanic plateau (Boher et al., 1992).

### 2.2. The Leo-Man Shield

The Leo-Man shield (Fig. 1b) is bounded to the east and west by Pan-African and Hercynian orogenic belts. It consists of the Archaean age Kénema-Man domain to the west and the Proterozoic Baoulé-Mossi domain to the east. The contact between the Archean and Proterozoic domains is marked by the Sassandra Fault (SF). The Baoulé-Mossi domain (also known as the Birimian domain) is located to the north and east of the Kénema-Man domain and characterized by extensively distributed N-S to NE-SW trending greenstone belts (the maximum length: 600–700 km), intruded and separated by several generations of granitoids, and/or by sedimentary basins. The Eburnean orogenic events, which shaped the crustal architecture in the Leo-Man shield operated from 2160 Ma to 1980 Ma (Davis et al., 1994; Feybesse et al., 2006). The first deformational event (D1), which operated between 2160 Ma and 2110 Ma (Baratoux et al., 2011; Ganne et al., 2012) is characterized by a major crustal thickening (Allibone et al., 2002; Vidal et al., 2009). The D2 deformational event continued up to 1980 Ma, where the initial D1 E-W compressional regime was switched to a dominant strike-slip transpression.

### 2.3. Summary of the BBT

The Paleoproterozoic BBT is in the eastern portion of the Baoulé-Mossi domain (Fig. 1c). The BBT consists of the NE-SW Bole-Nangodi shear zones, the N-S trending Wa-Lawra belt, the NNW trending Jirapa and the adjacent Jang shear zones, the E-W trending Julie belt, the northern Koudougou-Tumu granitoid domain, the central BBT, the southern Abulembire domain and the southeastern Maluwe basin (Fig. 1c, Block et al., 2015). The E-W-oriented Julie belt separates the Koudougou-Tumu granitoid domain from the BBT, and mostly consists of basalt, volcano-sedimentary rocks and granitoids (Amponsah et al., 2015). To the west of the Julie belt is the NNW trending Jirapa and its adjacent Jang shear zones, which separates the Koudougou-Tumu granitoid domain from the Wa-Lawra belt. The Jirapa shear zone merged with the southern portion of the Bole-Nangodi shear zones during extension (Block et al., 2015). The NE-SW Bole-Nangodi shear zones extend into the southern portion of Burkina Faso for over 300 km (Naba et al., 2004) and is composed of volcanic rocks, greywackes, shales, gabbros and deformed to undeformed granitoids with crystallization ages ranging from 2195 Ma to 2119 Ma. These rocks have been metamorphosed up to greenschist to amphibolite facies (De Kock et al., 2011).

Pressure-Temperature (PT) paths show a near-isothermal decompression (Fig. 2) during the D2, which took place between 2137 ± 8 Ma and 2127 ± 7 Ma (U-Pb, Block et al., 2015). This indicates an exhumation driven by extension on a magnitude

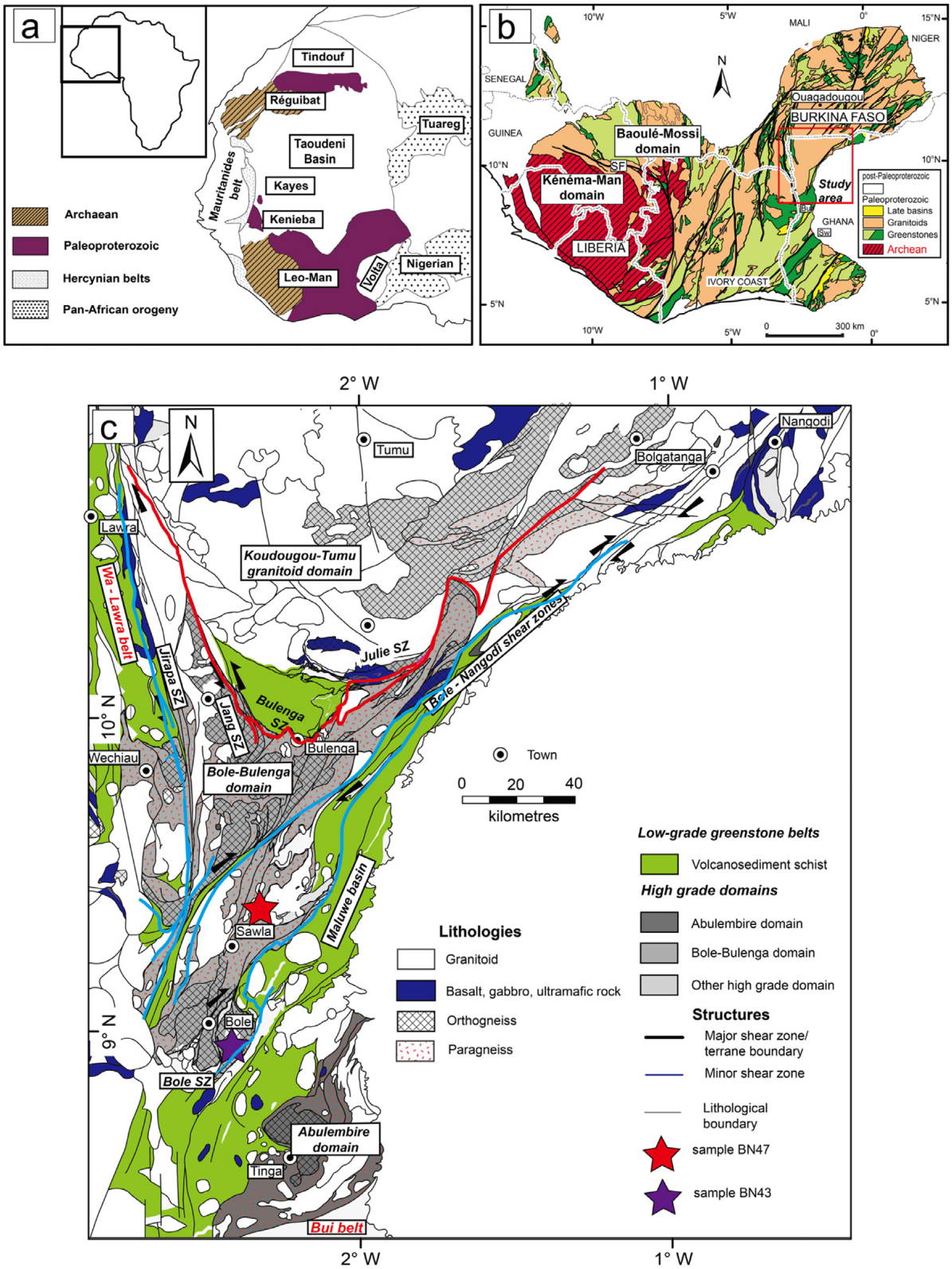


**Fig. 1.** (a) Sketch map of the WAC after Peucat et al. (2005). (b) Main geological units in the Leo-Man Shield. (c) The high-grade BBT after Block et al. (2015). Purple and red stars are used to show PT-paths in Figure 2.

order of cm/year (e.g., Rey et al., 2009). The maximum pressures calculated from paragneiss samples at the beginning of the D2 decompression range 11–13 kbar (corresponding to a depth of about 45 km).


https://doi.org/10.1007/s12303-019-0005-z

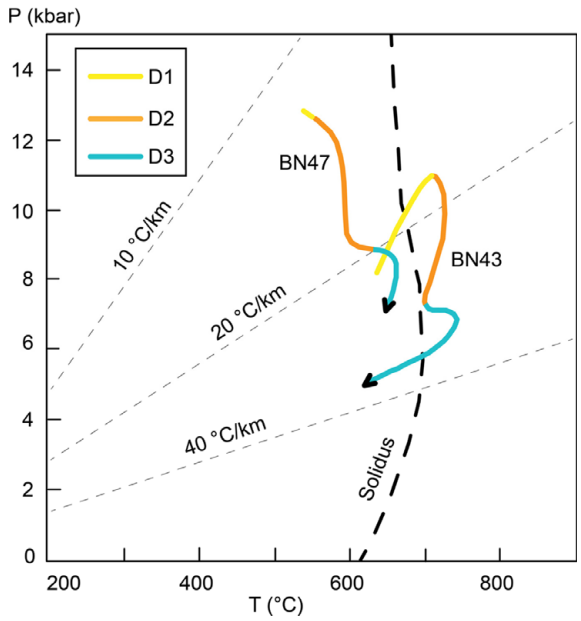


**Fig. 2.** PT-paths after Block et al. (2015). BN43 is a migmatitic paragneiss from the Bole-Nangodi shear zones. BN47 is a sample of paragneiss from the Bole-Bulenga domain.

## 3. MODEL DESCRIPTION AND ASSUMPTIONS

The numerical models were designed to show how the three pre-existing major shear zones involved in the BBT locally control the exhumation of the lower crustal materials under extension conditions, thus the probable conditions that existed during the D2 extension phase in BBT. The numerical code *Underworld* (bleeding edging version, 2015) utilized for the modelling, employs a Lagrangian Particle in cell finite element scheme (Moresi et al., 2003, 2007). The governing equations of momentum, mass and energy using the Boussinesq approximation are expressed as (De Smet et al., 1998; Moresi et al., 2003, 2007; O'Neill et al., 2016);

$$\tau_{i,j,j} - p_{,i} = f_i\,, \tag{1}$$

$$v_{i,i} = 0\,, \tag{2}$$

$$\frac{\partial T}{\partial t} + v \cdot \nabla T = k\nabla^2 T + \frac{H}{Cp} - \frac{lh}{Cp} \cdot \frac{\partial M}{\partial t}\,, \tag{3}$$

where $\tau$ is the deviatoric stress tensor, $p$ is the pressure, $v$ is the

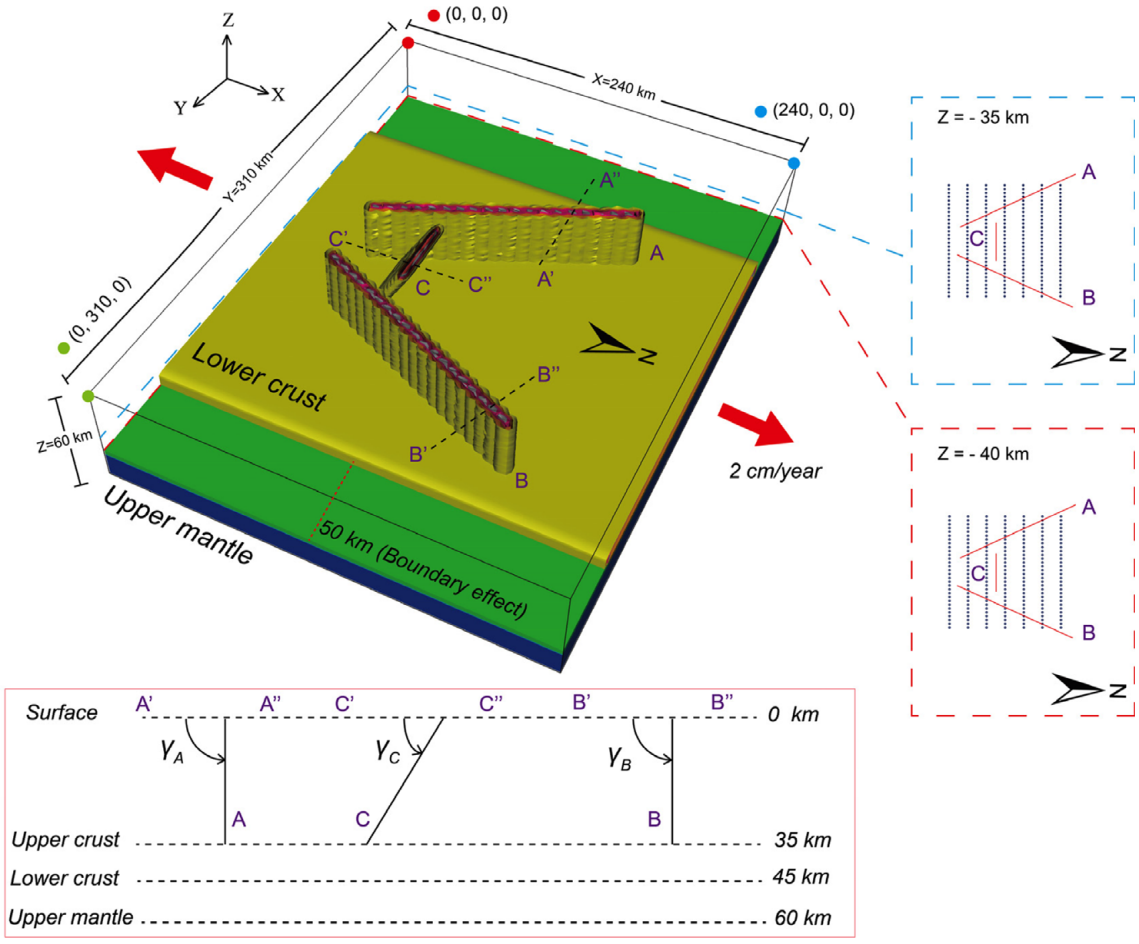


**Fig. 3.** Initial geometry and boundary conditions of the numerical model. The 3D model consists of three pre-existing faults in the upper crustal domain (Table 1). The azimuth of faults A, B and C are fixed to 335°, 25° and 90°, respectively. To the east and west of faults, a 50 km wide distance is employed to reduce the boundary effect. The angles $\gamma_A$, $\gamma_B$ and $\gamma_C$ are counted counterclockwise from surface to faults A, B and C, indicated by the cross-sections A'–A", B'–B" and C'–C". 420 passive particles are placed in the horizontal planes of Z = –35 and –40 km.

velocity, $f_i$ is a body force, representing gravity in the vertical direction, $k$ is the thermal diffusion, $H$ is the radiogenic heat production per mass unit, $Cp$ is the heat capacity, $lh$ is the latent heat and $M$ is the melt fraction (Table 2).

The initial geometry for the present study were restricted to a 3D Cartesian volume (Figs. 3 and S1 (Electronic supplementary material)), with a 60 km maximum thickness (this thickness includes the upper mantle according to the geophysical signatures by Jessell et al., 2016), 310 km horizontal length (YY direction), 240 km wide (XX direction) and a 35 km (ZZ direction) non-Newtonian rheological layer (creep power law exponent can be found in Table 3). A 10 km non-Newtonian lower crust is defined below the upper crust. Beneath the lower crust, a 15 km non-Newtonian upper mantle defines the base of the model. In the lower crust, 420 passive particles are placed at depths Z = –35 km and –40 km to track displacements. This model is modelled as a visco-plastic rheology. This version of *Underworld* did not allow the use of elastic properties, some paper has contributed to explore the role of viscoelasticity in modelling lithospheric instability (So et al., 2012, 2014; Farrington et al., 2014), but in our paper its effect on deformation does not significantly influence the results since materials yield rapidly (Ellis et al., 2004; Buiter et al., 2007). The effective viscosity varies with the temperature and stress is calculated with a non-Newtonian power law (Ganne et al., 2014):

$$\eta_0 = 0.25 \cdot (0.75A)^{(-1/n)} \cdot \dot{\varepsilon}^{((1/n)-1)} \cdot \exp^{(Q/nRT)}, \quad (4)$$

where A is the dislocation creep law pre-exponential factor, n is the dislocation creep law exponent, Q is the activation energy, $\dot{\varepsilon}$ is the strain rate.

The displacement boundary condition for extension is programmed at a rate of 2 cm/year for each side in XX direction. The upper mantle can flow in at a normal velocity (free slip in horizontal direction) to balance the volume reduction per time step (automatically calculated according the applied extensional velocity) due to extension (Liao and Gerya, 2014). A depth dependent Drucker-Prager yield criterion is employed to model the deformation behaviour, which is expressed as follows (Sharples et al., 2015):

**Table 1.** 3D Experiments with different orientations

| Experiment 3D# | $\gamma_A$/(°) | $\gamma_C$/(°) | $\gamma_B$/(°) | Stretching Factor (SF) |
|---|---|---|---|---|
| 3D-a | 90 | 60 | 90 | 5.8% |
| 3D-b | 90 | 120 | 90 | 5.5% |
| 3D-c | 120 | 60 | 60 | 5.3% |
| 3D-d | 120 | 120 | 60 | 5.6% |
| 3D-e | 120 | 30 | 60 | 5.4% |
| 3D-f | 120 | 150 | 60 | 5.2% |
| 3D-g | 120 | 120 | 120 | 5.1% |
| 3D-h | 60 | 120 | 120 | 5.2% |
| 3D-i | 90 | No fault | 90 | 7.0% |
| 3D-j | 120 | No fault | 60 | 6.4% |

$$\tau_{II} = \delta_c + P \cdot tan\varphi, \quad (5)$$

where $\tau_{II}$ is the second invariant of the deviatoric stress tensor, $P$ is the local pressure and $\varphi$ is the internal friction angle. An initial cohesion and coefficient of friction of 15 MPa and 0.44 respectively for the crust and mantle domain were employed, whilst pre-existing faults are set to 10% of the initial values. For the crust and mantle domains, a strain-weakening principle (Gueydan et al., 2014) is applied to model the effective cohesion and coefficient of friction angle (drop to a maximum of 20%, Collettini et al., 2009). Shear heating was not considered in brittle and ductile domains (e.g., Mulchrone and Mukherjee, 2015; Mukherjee, 2017; Mukherjee and Khonsari, 2017, 2018; Mukherjee and Agarwal, 2018) that otherwise could have affected the deformation/flow.

With respect to thermal conditions (Mukherjee, 2017), the model is subjected to a "hot" lithospheric extension conditions, with a crust of 45 km (geophysical signatures from Jessell et al., 2016) and a Moho temperature of about 900 °C (Tirel et al., 2008; Wang et al., 2015), assuming a geothermal gradient of 20 °C/km. The temperatures at the surface and bottom are fixed to 20 °C and 1220 °C respectively, similar to the temperature conditions described by Ganne et al. (2014). Regarding the partial melting for the crustal layers, rocks of the upper crust are characterized by low rate of melt yield and hence starts melting at a relatively high solidus temperature of $T_{sol}$ = 836 °C (Ganne et al., 2014). These conditions correspond to a buried depth of about 40 km assuming a temperature gradient of 20 °C/km. In this study, the thickness of upper crust is set to 35 km, with an extensional boundary condition and based on this model setup as well as thermodynamic assumptions, only the lower crust can melt. The volumetric melt fraction for the lower crust is calculated according to the procedures outlined by Gerya and Yuen, (2003). The volumetric melting coefficient ($X_M$) for calculating melt fraction ($M$) is expressed as Equations (6) and (7):

$$\begin{aligned} X_M &= 0 \quad \text{at } T \le T_{sol}, \\ X_M &= \frac{T - T_{sol}}{T_{liq} - T_{sol}} \quad \text{at } T_{sol} < T < T_{liq}, \\ X_M &= 1 \quad \text{at } T \ge T_{liq}, \end{aligned} \quad (6)$$

where $T_{sol}$ and $T_{liq}$ are the wet solidus and dry liquidus temperatures of the lower crust, respectively. We assume that the $T_{sol}$ and $T_{liq}$ temperatures do not change with pressure (Gerya et al., 2008; Ganne et al., 2014; Feng et al., 2018a, 2018b).

In the present study, we generally followed the deductions drawn by Gerya et al. (2008) and Ganne et al. (2014) that, when the temperature is above the wet solidus temperature and below the dry liquidus temperature the volumetric melt fraction ($M$) increases linearly with temperature:


https://doi.org/10.1007/s12303-019-0005-z

**Table 2.** Thermo-mechanical model parameters, symbol and value-units

| Parameter | Symbol | Value-units |
|---|---|---|
| Thickness | $H_{upper}$ | 35 km |
| | $H_{lower}$ | 10 km |
| | $H_{mantle}$ | 15 km |
| Density | $\rho_{upper}$ | 3050 kg/m$^3$ |
| | $\rho_{lower}$ | 2700 kg/m$^3$ |
| | $\rho_{mantle}$ | 3250 kg/m$^3$ |
| | $\rho_{fault}$ | 2800 kg/m$^3$ |
| Melting point of lower crust (Ganne et al., 2014) | $T$ | $T_{sol}$ = 636 °C (1%), $T_{liq}$ = 1200 °C (80%) |
| Heat capacity | $Cp$ | 1000 J/kg·K |
| Thermal diffusivity | $k$ | $10^{-6}$ m$^2$/s |
| thermal expansion coefficient | $\alpha$ | $3 \times 10^{-5}$ K$^{-1}$ |
| Latent heat | $lh$ | 300 KJ kg$^{-1}$K$^{-1}$ |
| Gas constant | $R$ | 8.314 J mol$^{-1}$ K$^{-1}$ |
| Gravitational acceleration | $g$ | 9.81 m/s$^2$ |
| Friction angle for Drucker-Prager criterion | $\varphi/f$ | 3–25° |
| Cohesion for Drucker-Prager criterion | $\delta_c$ | 3–15 MPa |

**Table 3.** Rheological parameters for different layers (Ranalli, 1995 and references therein)

| Layer | Rock type | A (MPa$^{-n}$/s) | n | Q (kJ/mol) |
|---|---|---|---|---|
| Upper crust | Diabase | $2.0 \times 10^{-4}$ | 3.4 | 260 |
| Lower crust | Quartzodiorite | $1.3 \times 10^{-3}$ | 2.4 | 219 |
| Uppermost mantle | Dry olivine | $7 \times 10^{4}$ | 3.3 | 520 |
| Fault | | | $10^{20}$ Pa s | |

The effective viscosity is calculated with a non-Newtonian power law: $\eta_0 = 0.25 \cdot (0.75A)^{(-1/n)} \cdot \dot{\varepsilon}^{((1/n)-1)} \cdot \exp^{(Q/nRT)}$.

$$M = X_M \cdot M_{max}. \tag{7}$$

When the temperature reaches the melting point of the lower crust ($T_{sol}$), a reducing factor is applied to model effective viscosity (Pinkerton and Stevenson, 1992), which is function of melt fraction $M$:

$$\eta_{eff} = 5 \times 10^{16} \cdot \exp\left(2.5 + (1-M)\left(\frac{1-M}{M}\right)^{0.48}\right). \tag{8}$$

The effective density in the computational domain is calculated according to the temperature and the thermal expansion coefficient ($\alpha$) of $3{\cdot}10^{-5}$ K$^{-1}$. A constant thermal diffusivity of $10^{-6}$ m$^2$/s is applied. To relate density to temperature, a linear relationship for the non-meltable layers (upper crust, upper mantle and fault domains) is expressed as:

$$\rho_{eff} = \rho[1 - \alpha(T - T_0)]. \tag{9}$$

For lower crust, we follow the *Underworld* module (LinearDensityMelt) to calculate the effective density. A more detail model can be set up by considering the concept of representative density (Mukherjee, 2017, 2018a, 2018b, 2018c), but is avoided for the time being. In our model, it is a function of temperature, melt fraction and pressure (similarly prescribed in Rey et al., 2009):

$$\rho_{eff} = \rho[1 - \alpha(T - T_0) - mc \cdot M + \beta(P - P_0)], \tag{10}$$

where $\rho_{eff}$ is the effective density, $\rho$ is the original density, $\alpha$ is the thermal expansion coefficient, $T$ is the local temperature, $T_0$ is the reference temperature at surface (20 °C), $mc$ is the coefficient of expansion related to phase change, $\beta$ is the compressibility coefficient ($10^{-11}$ Pa$^{-1}$, similar to Ganne et al., 2014), $P$ is the local pressure and $P_0$ is the reference pressure.

## 4. RESULTS

The outcome from the numerical solutions to the problem of how the orientation of pre-existing faults influence exhumation (decompression from 11–13 kbar to 6–7 kbar) of lower crustal materials were tested using ten 3D models. All models were run on the EOS cluster in Toulouse. We map the accumulation of the second invariant ($\varepsilon_{II}$) of the strain rate (*EII* shearing strain, calculated by $EII = \sum_0^t \varepsilon_{II} \cdot \Delta t$) and N-S ($\varepsilon_{xx}$) strain rate over time (*Exx* extensional strain, calculated by $Exx = \sum_0^t \varepsilon_{xx} \cdot \Delta t$) to show the potential/preferential channels for further emplacement.

### 4.1. 3D Model for the Exhumation of the Lower Crust

For experiments 3D-a and 3D-b (Figs. 4a and b), faults A and

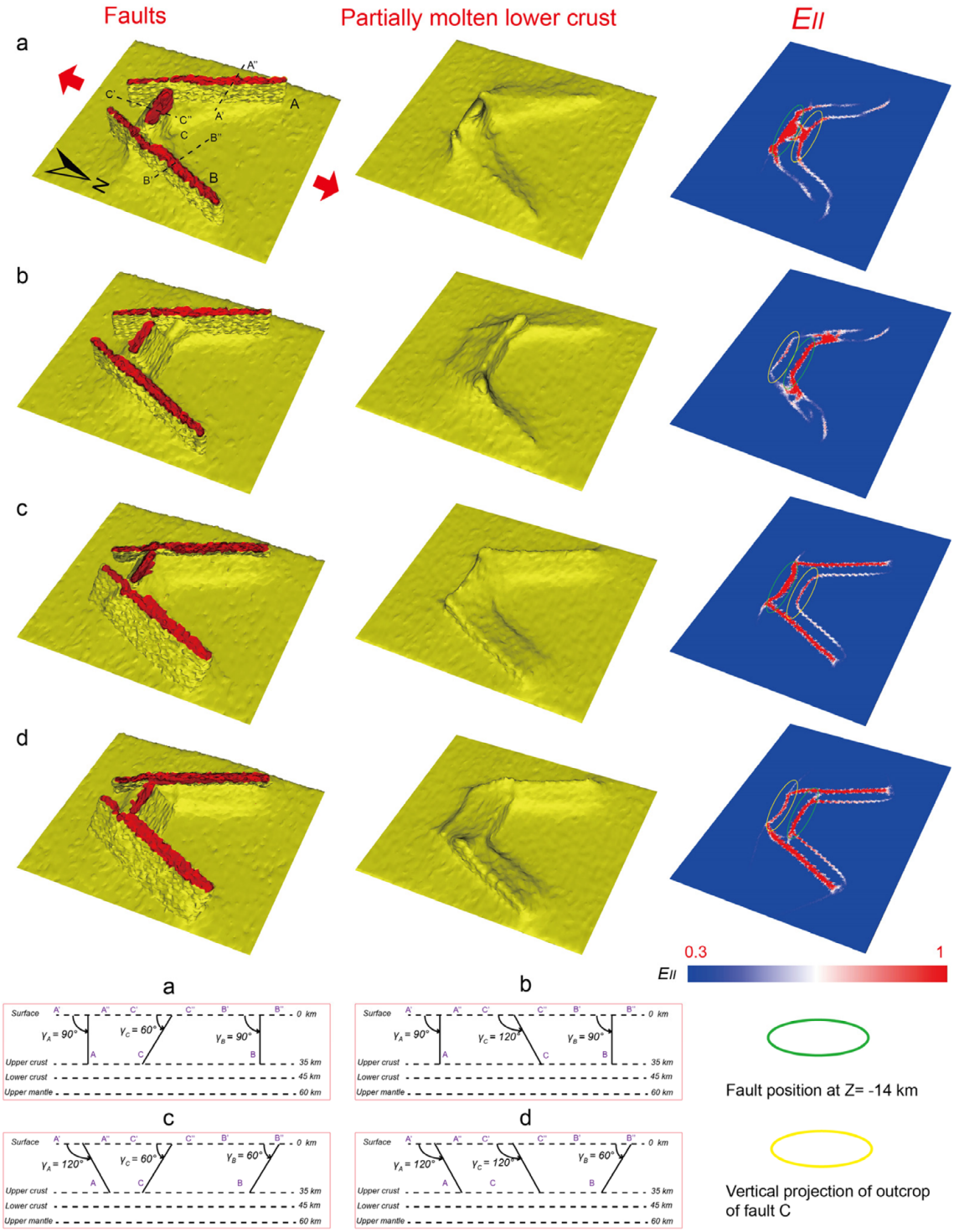


**Fig. 4.** Influence of the orientation of faults on exhumation of the partially molten lower crust. The faults and the upper surface of the partially molten lower crust are plotted in the first column in yellow, the upper surface (outcrops) of the faults are indicated in red. The relief of the upper surface of the partially molten lower crust alone is plotted in the second column. In the third column *EII* is shown (sections in column three at a depth of Z = –14 km), which is the accumulation of the second invariant of the strain rate ($\varepsilon_{II}$) over time (calculated by $EII = \sum_0^t \varepsilon_{II} \cdot \Delta t$).

B were both set to vertical ($\gamma_A = \gamma_B = 90°$, Fig. 3, Table 1), and the dip of fault C was set to $\gamma_C = 60°/120°$, respectively. Partially molten rocks from the lower crust advance towards and concentrate along the pre-exiting faults A, B and C driven by density contrasts and viscosity changes. Both experiments showcase the non-identical nature of models with varying fault dips, pertaining to


https://doi.org/10.1007/s12303-019-0005-z

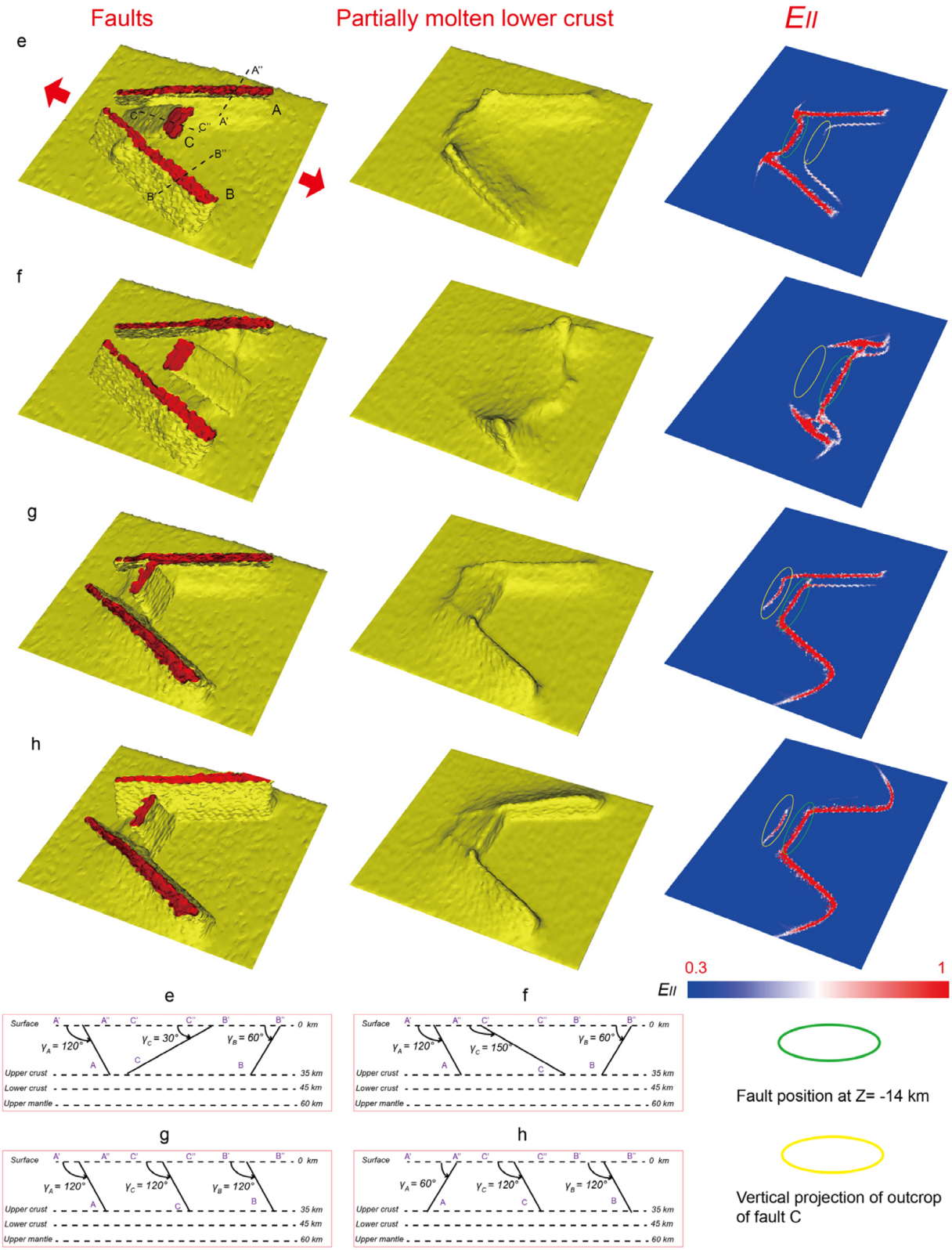


**Fig. 4.** (continued).

the distribution of molten rocks focused on the southern portions of each model with high concentration of molten rocks along the footwall of fault C. This phenomenon will allow and increase the surge of partial molten material through fault C as the stretching factor increases due to continuous extension and permits the emplacement of these molten materials at shallower depths of

the hanging wall.

Symmetrically inclining faults A and B at angles $\gamma_A = 120°$ and $\gamma_B = 60°$, and that of the dip of fault C at $\gamma_C = 60°/120°$ (Figs. 4c and d) and 30°/150° (Figs. 4e and f) respectively, partially molten rocks tend to focus along the footwalls of faults A, B and C during extension. The concentration of partially molten lower crustal materials is greater, when the dip of fault C is fixed at $\gamma_C = 60°/120°$ than when fixed at $\gamma_C = 30°/150°$. With regards to experiments 3D-e and 3D-f, the dips of fault A and B were fixed to $\gamma_C = 60°/120°$ and that of fault C is $\gamma_C = 30°/150°$ (Figs. 4e and f). The results of this experiment demonstrate that, the exhumation of lower crustal materials is more significant along the footwalls of faults A and B than that along the footwall of fault C during extension (Fig. 4). This indicates that, within a fault system, dip angles of faults and their relative positions jointly control the concentration and distribution of partially molten lower crustal materials during extension.

### 4.2. 3D Model for the Finite Strain

The horizontal cross sections of finite strain at Z = –14 km show the accumulations of shear (Fig. 4) and extensional (Fig. S2 (Electronic supplementary material)) strains. Areas of extension mainly focus at the fault C, that is because the strike of fault C is perpendicular to the direction of extension, and therefore results is a larger local extension and thinning of the upper crust. In Figure 4, double bounded finite strain belts (the red color in the third column in Fig. 4) are observed in models 3D-a~3D-f. Thus, an initial belt is evolved from a pre-existing fault whilst, the other is newly formed during exhumation of lower crustal materials along the boundaries of pre-existing faults.

In model 3D-h, faults A and B are symmetrically inclined at $\gamma_A = 60°$, $\gamma_B = 120°$. The experiment only exhibits a high-strain belt with tips reaching the eastern and western boarders of the models. For the asymmetric system (Fig. 4g), one of the tips of high-strain belt reaches the eastern border of the model. This is due to the fact that partially molten rocks in models 3D-h and 3D-g concentrate preferentially along the external boundaries of faults A and B (along the footwalls of faults A and B). The travel distance for partially molten crustal materials to the eastern and western borders of the model is decreased so that the boundary effect is probably amplified.

## 5. DISCUSSION

### 5.1. Distribution of Lower Crustal Materials

The orientation of pre-existing faults, geothermal gradient and thickness of the lithosphere (Wang et al., 2015) all play important roles in influencing the evolution and distribution of lower crust exhumation during extension. With respect to an over-thickened continental crust in extension, Rey et al. (2009) numerically modelled a normal fault with a specific dip angle (45°) in the homogeneous upper crust. In their models, the domes

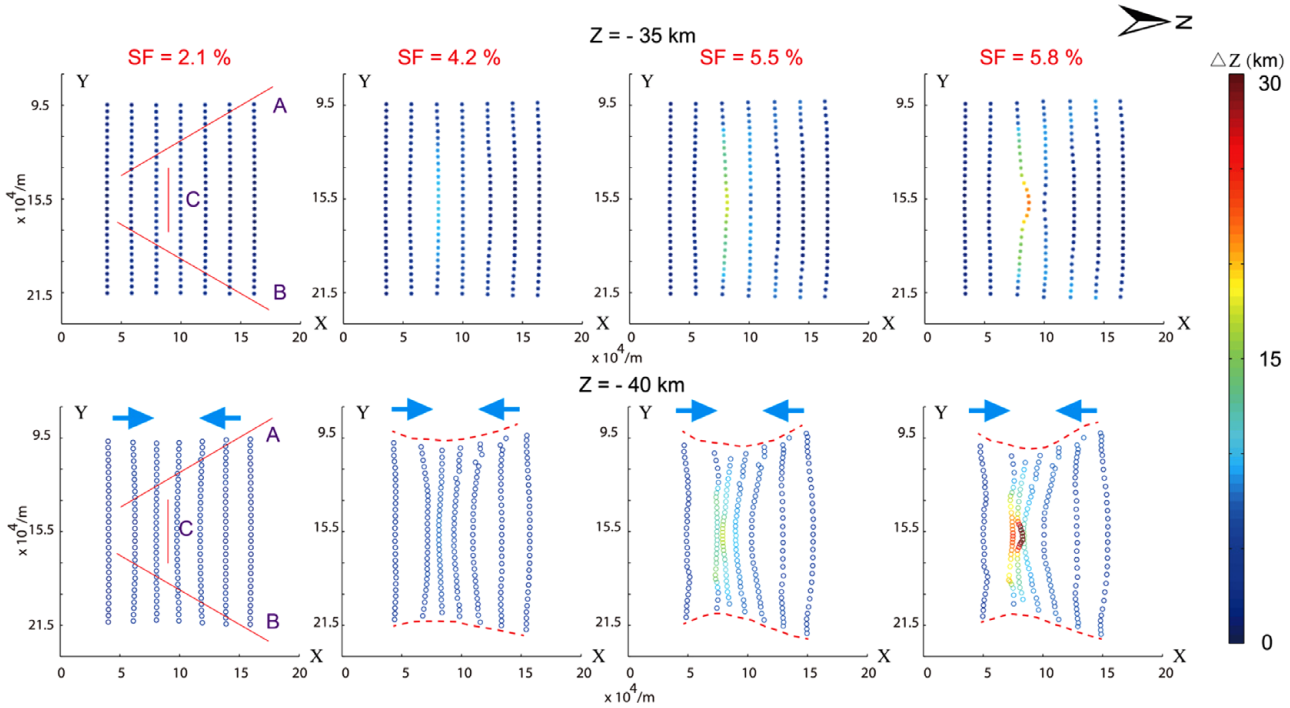


**Fig. 5.** The tracks and exhumation of passive particles in the lower crust. SF represents the N-S Stretching Factor (Table 1). The color bar represents the uplifted height of particles during extension.


https://doi.org/10.1007/s12303-019-0005-z

of partially melting low crust always remain at the footwall of the normal fault for different rates of extension. In the analogue models of Brun et al. (1994) and Sokoutis et al. (2007), the role of location and orientation of weak heterogeneities in the extension of sandbox models were tested and correlated well with the wide rifting mode of extension found in numerical modelling (Rey et al., 2009, 2011). Wang et al. (2015) explored the conditions of MCCs formation in a non-over-thickened continent crust (35 km thick). They demonstrated that a high local geothermal gradient, a weak ductile lower crust and a slow extension rate can also result in the formation of MCCs. Rey et al. (2017) show a set of 3D experiments mapping the flow of the lower crust in a pull-apart region bounded by two verticals strike-slip faults.

To quantify the effect of buoyancy in the upward flow of partially molten lower crustal materials, we plot the paths of two groups of passive particles (Z = –35 km and –45 km) at different stretching factors (Fig. 5) for model 3D-a. The exhumation of lower crust occurs at a relatively low rate prior to SF = 4.2%, and the major exhumation takes place later as extension continues. The reason for the lag is probably due to the resistance to deformation and the effect of strain weakening (Wang et al., 2015; Feng et al., 2016b). This also can be explained by the findings of Huismans and Beaumont (2002): their results show that the lithospheric extension commonly has a two-phase spatial-temporal development over a wide range of extension rates (from 0.3 to 30 cm/year). The first one is mainly controlled by frictional behaviour and the second phase is controlled by ductile rheology.

In upper and middle planes of lower crust, density and viscosity contrasts resulting from increasing temperature, viscosity and melting fraction (Ganne et al., 2014) and the role of extension rate significantly influence the path of particle flow. The shallower passive particles (Fig. 5) are less sensitive to extension as they are mechanically constrained by the competent upper crust and relatively lower ambient temperature, without considering wet quartzite law for crustal behaviour. The deeper passive particles tend to move towards the center of the model (up to 20 km, indicated by the blue arrows), which is associated with significant exhumation between the nearly-intersecting-zones (dextral opening zipper) of the pre-existing faults (Platt and Passchier, 2016; Passchier and Platt, 2017).

## 5.2. Distribution of Finite Strain

High-strain zones play an important role in the emplacement of partially molten rocks (e.g., Neves et al., 2000; Weinberg et al., 2009). In order to examine the contribution of lower crust exhumation

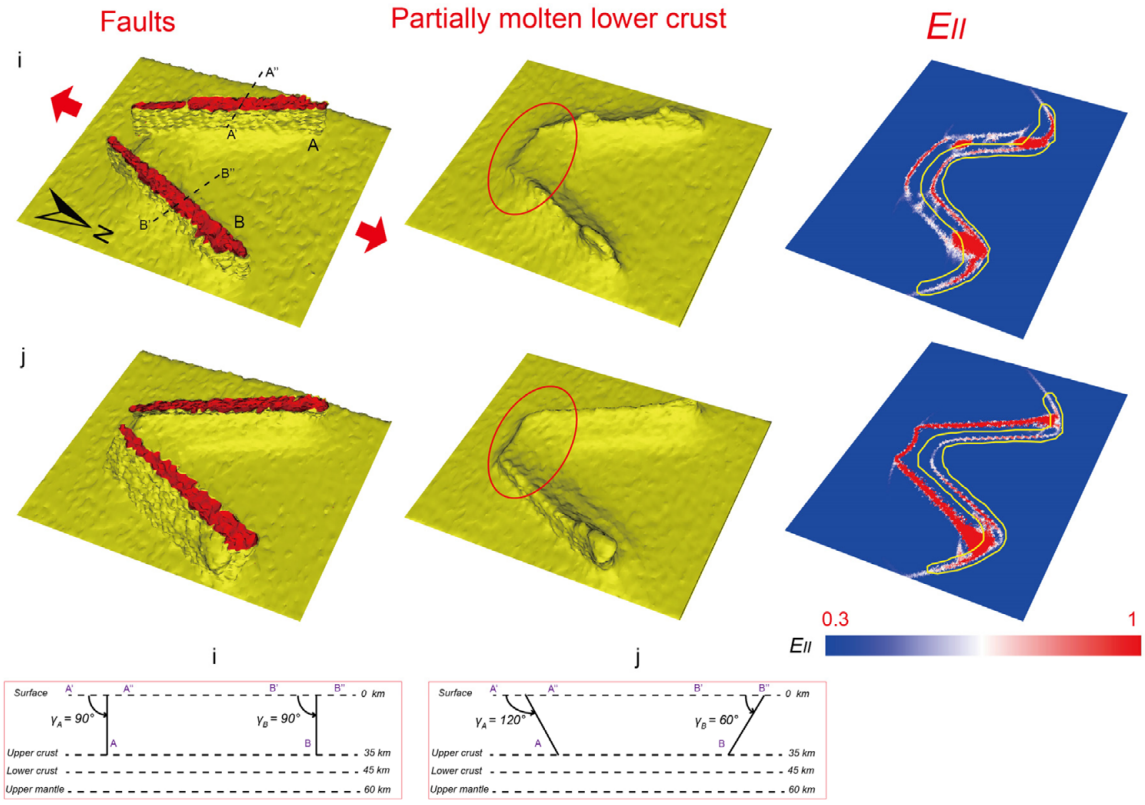


**Fig. 6.** Model domain consists of two pre-existing faults. The faults and the upper surface of the lower crust are plotted in the first column in yellow, the upper surface (outcrops) of the faults are indicated in red. The relief of the upper surface of the partially molten lower crust alone is plotted in the second column. Yellow lines are used to indicate the newly produced high-strain belt during N-S extension (at a depth Z = –14 km).

from different faults, and to further explore the influence of pre-existing faults pertaining to the evolution and formation of high-strain zones, the 3D model is simplified by discarding fault C (Fig. 6). Double finite strain belts similar to experiments 3D-a~3D-f are observed. Generally, pre-existing faults requires a lateral velocity discontinuity and operates as a localization factor for deformation (Le Pourhiet et al., 2004). During extension, pre-existing faults are easily reactivated (Dasgupta and Mukherjee, 2017) and tend to concentrate high-strain. This is due to the varying rheological heterogeneity and mechanical anisotropy of the strained materials compared to their surrounding rocks. The processes of concentrating strain into pre-existing faults developing one of the two finite strain belts (the zone not bounded by a yellow solid line in Fig. 6).

Along the internal boundaries of the high-strain belt, a new high-strain belt is formed (bounded by yellow solid lines in Fig. 6). This second belt is conjugated of the first belt and initiates at the line of contact between the base of the pre-existing fault and the lower crust. During extension, partially molten materials from the lower crust tend to be exhumed along the footwalls of pre-existing faults. The upward flow of partially molten rocks weakens and reduces the strength of the overlying rocks due to an increment ambient temperature gradient. Therefore, the probable mechanisms associated with the formation of such high-strain belts (bounded by yellow lines in Fig. 6) are from the combination of deformation and localized upwelling partially molten rocks along the footwalls of pre-existing faults during extension.

Comparing the newly formed belts in experiments 3D-i and 3D-j, the width of the belts segment located in the intersection of faults is wider in experiment 3D-i (Fig. 6i). This indicates the dips of fault play a significant role in influencing the relative position of the formation of these high-strain belts. According to the spatial relationship and distribution of partially molten lower crustal materials and high-strain belts (Figs. 4 and 6), the exhumation of partially molten rocks is almost bounded by the two high-strain belts, resulting in the formation of high-grade rocks corridors in the models (trapezoid-shape in Fig. 6).

When the fault system does not include fault C (Fig. 6), the concentration of partially molten lower crust at the southern nearly-intersecting region of the pre-existing faults is still observed (red ellipses). This is due to the increasing concentration of partially molten lower crust along pre-existing faults as the space between faults A and B narrows from north to south.

## 5.3. Model Implications for the BBT

Identifying and exploring the spatial distribution and relationship of structures helps in constraining the evolution of deformation and exhumation of lower crust in the BBT during the Eburnean orogeny. The sketch in Figure 7a shows the probable evolutionary history of main structures in the BBT based on this work. During the D2 N-S extension, newly-formed high-strain belt bounded by faults A and B overlaps with the inherited fault C. The mechanisms for the formation of these new high-strain belts are probably from a combined contribution of mechanical deformation of pre-existing faults and emplacement of upwelling partially molten rocks along faults.

The high-strain corridors (designated by black ellipses in Fig. 7a) are defined by the inherited and newly formed structures which aids in the channelization process of partially molten

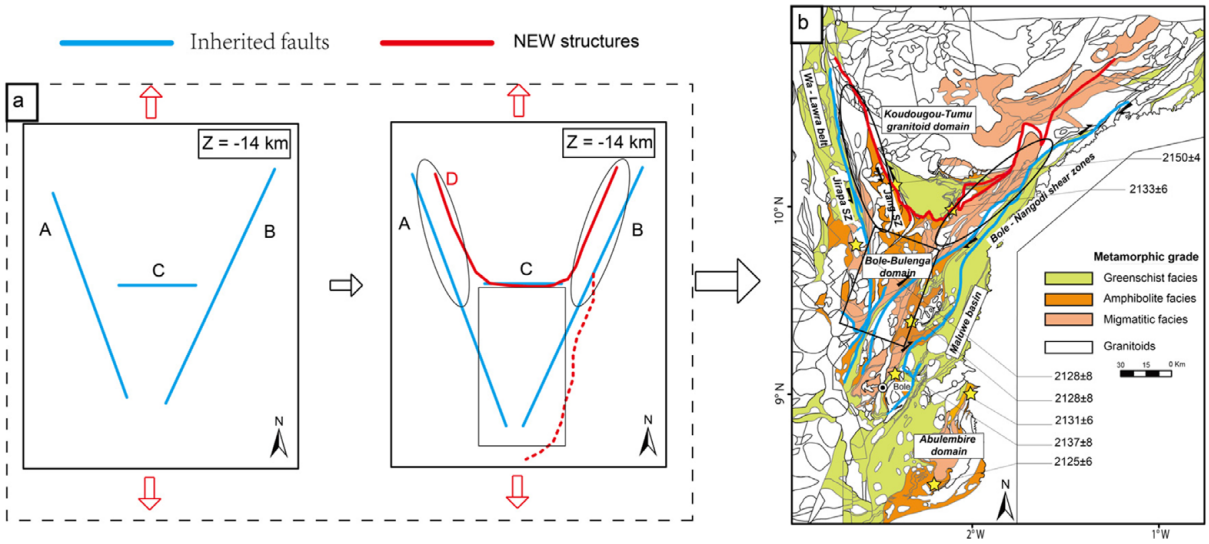


**Fig. 7.** (a) Sketch showing the evolution of main structures (Z = –14 km, pressure is about 4–5 kbar, corresponding to the pressure at the end of D3 stage, Fig. 2). Faults A, B and C are thought to be inherited structures. During the N-S extension, a new high-strain belt (red solid line in Fig. 7a) will be produced and bounded by pre-existing faults A and B. Fault C provides initial weak sites for concentrating strain, and as a result, the newly formed high-strain belt would overlap with fault C. (b) Metamorphic map after Block et al. (2015).


https://doi.org/10.1007/s12303-019-0005-z

materials. This process is supported and evidenced by the elevated concentration of partial molten rocks along pre-existing faults (Fig. 4) and the exhumation of partially molten rocks from lower crustal sources into upper crust along high strain zones (Neves et al., 1996, 2000; Weinberg et al., 2009).

In NW Ghana, high-strain zones (represented by red and blue lines in Fig. 7b) separate high-grade rocks (up to amphibolite to migmatite facies) from adjacent lower grade greenstone belts. In the eastern and western parts of the high-grade rock corridors (black ellipses in Fig. 7b), the high-grade rocks exhumed from the lower into middle crustal levels (possibly to the upper crust) would be facilitated by these km-scale high-strain corridors (designated by black ellipses in Fig. 7a). In the central part of the BBT (black box in Fig. 7b), the high-grade rocks are exhumed under a coupling assistance related to the main structures. Therefore:

(1) Increasing exhumation of partially molten rocks with the narrowing space from north to south between the Jirapa and Bole-Nangodi faults (faults A and B in Fig. 7a)

(2) Inherited orthogonal (E-W) structures (fault C in Fig. 7a) would significantly increase the exhumation of lower partially molten rocks in the central part (Fig. 4), otherwise partially molten rocks would have been difficultly exhumed and have hardly formed such high concentration of exhumation (Fig. 7) in the study area in the center of the BBT.

Extensional processes that predated the D3 event significantly contributed to exhumation of deep partially molten rocks in the BBT. The numerical results indicate that the processes of exhumation involve fast movements (kyr-scale) under the assistance of pre-existing shear zones, that is three magnitude orders lower compared to the Myr-scale encompassing the Eburnean events (2.15 to 2.10 Ga).

### 5.4. Limitations and Perspectives

Although we have stated that the elastic deformation does not significantly influence the results, since the materials yield at small strains (Ellis et al., 2004; Buiter et al., 2007), it would be useful to exploit this when elastic modulus responsible for this is added to Underworld (So et al., 2012, 2014; Farrington et al., 2014). Since we focus here on discussing the influence of orientation of faults in exhumation of the lower crust, only the upper part of the lithosphere is modelled (60 km), the whole lithospheric scale modelling is not thought to substantially influence the result but could be included in the future. Further geophysical (Jessell et al., 2016) and geochemical (Ganne et al., 2016; Ganne and Feng, 2017, 2018) constraints (Moho depth, geochronological data, viscosity of rocks, stretching rate) could be included to optimize the setup of the model. In this study, we only model an episodic N-S extensional process (D2) by assuming the thickened thickness of crust at the end of D1. It will be significant to model a continuous deformation process by including crustal thickening during D1 and subsequent D2 extension. In addition, in our model we employed constant solidus and liquidus temperatures for the partially melting lower crust, it may cause abnormally larger amount of melt and obtain a low viscosity when the pressure difference is huge, it would be great to relate pressure to the temperatures for obtaining realistic solidus and liquidus temperatures.

With respect to the investigated development of the late exhumation of the Tauern Window (dominated by strike-slip and extensive regimes within the Tauern Window and along its borders), Eastern Alps, they propose a two-stage deformation history in order to explain the different types of structures (Bertrand et al., 2015). In the first stage, the Tauern Window was dominated by N-S shortening and compression, after that, the main stage responsible for exhumation was marked by normal faulting at the borders of the dome and strike-slip faulting in the core.

## 6. CONCLUSIONS

We built ten 3D thermo-mechanical models to explore the influence of pre-existing faults on the lower crust exhumation in extension in the explicit context of BBT in NW Ghana. The exhumation of lower crust occurs at a relatively low rate prior to SF = 4.2%, and the major exhumation takes place later. The partially molten lower crust rocks tend to move towards the center of the model (up to 20 km) and focus exhumation around the near-intersection-zones of pre-existing faults.

The high-strain corridors observed in the numerical models can be used to explain the loci of exhumation of the lower crust in NW Ghana during the D2 N-S extension. In the eastern and western parts of the corridors in NW Ghana, high-grade rocks exhumed from the lower to middle crustal level (possibly to upper crust) would be facilitated by these km-scale high-strain corridors. In the central part of the BBT, the high-grade rocks are exhumed resulting from a coupling between: (1) The exhumation of partially molten rocks between the faults Jirapa and Bole-Nangodi would increase due to the reduction in space from north to south. (2) Inherited orthogonal (E-W) structures would significantly increase the quantity of partially molten rocks, as otherwise partially molten rocks would have been hard to exhume in the center of the BBT.

## ACKNOWLEDGMENTS

This project is supported by "the Fundamental Research Funds for the Central Universities" (2018QNB01) and funded by the Priority Academic Program Development of Jiangsu Higher Education Institutions (PAPD). Laetitia Le Pourhiet, Laurent

Jolivet and Patrice Rey are thanked for constructive comments on the earlier version of this paper. Editor Sanghoon Kwon, Bokyun Ko, and two anonymous reviewers are warmly thanks for providing very constructive reviews.

## REFERENCES

Allibone, A., Teasdale, J., Cameron, G., Etheridge, M., Uttley, P., Soboh, A., and Lamb, E., 2002, Timing and structural controls on gold mineralization at the Bogoso gold mine, Ghana, West Africa. Economic Geology, 97, 949–969.

Amponsah, P.O., Salvi, S., Béziat, D., Siebenaller, L., Baratoux, L., and Jessell, M.W., 2015, Geology and geochemistry of the shear-hosted Julie gold deposit, NW Ghana. Journal of African Earth Sciences, 112, 505–523.

Baratoux, L., Metelka, V., Naba, S., Jessell, M.W., Grégoire, M., and Ganne, J., 2011, Juvenile Paleoproterozoic crust evolution during the Eburnean orogeny (~2.2–2.0 Ga), western Burkina Faso. Precambrian Research, 191, 18–45.

Bellahsen, N. and Daniel, J.M., 2005, Fault reactivation control on normal fault growth: an experimental study. Journal of Structural Geology, 27, 769–780.

Bertrand, A., Rosenberg, C., and Garcia, S., 2015, Fault slip analysis and late exhumation of the Tauern Window, Eastern Alps. Tectonophysics, 649, 1–17.

Block, S., 2015, Evolution géodynamique du craton Ouest Africain au nord du Ghana. Ph.D. Thesis, Université Toulouse III-Paul Sabatier, Toulouse, 359 p.

Block, S., Ganne, J., Baratoux, L., Zeh, A., Parra-Avila, L., Jessell, M., Ailleres, L., and Siebenaller, L., 2015, Petrological and geochronological constraints on lower crust exhumation during Paleoproterozoic (Eburnean) orogeny, NW Ghana, West African Craton. Journal of Metamorphic Geology, 33, 463–494.

Block, S., Jessell, M., Aillères, L., Baratoux, L., Bruguier, O., Zeh, A., Bosch, D., Caby, R., and Mensah, E., 2016, Lower crust exhumation during Paleoproterozoic (Eburnean) orogeny, NW Ghana, West African Craton: interplay of coeval contractional deformation and extensional gravitational collapse. Precambrian Research, 274, 82–109.

Boher, M., Abouchami, W., Michard, A., Albarede, F., and Arndt, N.T., 1992, Crustal growth in West Africa at 2.1 Ga. Journal of Geophysical Research: Solid Earth, 97, 345–369. https://doi.org/10.1029/91JB01640

Brun, J.P., Sokoutis, D., and Van Den Driessche, J., 1994, Analogue modeling of detachment fault systems and core complexes. Geology, 22, 319–322.

Buiter, S.J. and Torsvik, T.H., 2007, Horizontal movements in the eastern Barents Sea constrained by numerical models and plate reconstructions. Geophysical Journal International, 171, 1376–1389.

Burg, J.P., Bodinier, J.L., Gerya, T., Bedini, R.M., Boudier, F., Dautria, J.M., and Balanec, J.L., 2009, Translithospheric mantle diapirism: geological evidence and numerical modelling of the Kondyor zoned ultramafic complex (Russian Far-East). Journal of Petrology, 50, 289–321.

Choi, E., Buck, W.R., Lavier, L.L., and Petersen, K.D., 2013, Using core complex geometry to constrain fault strength. Geophysical Research Letters, 40, 3863–3867.

Collettini, C., Niemeijer, A., Viti, C., and Marone, C., 2009, Fault zone fabric and fault weakness. Nature, 462, 907–910.

Coney, P.J., 1980, Cordilleran metamorphic core complexes: an overview. In: Crittenden, M.D. Jr., Coney, P.J., and Davis, G.H. (eds.), Cordilleran Metamorphic Core Complexes. Geological Society of America, Memoirs, 153, p. 7–31.

D'Agostino, N., Chamot-Rooke, N., Funiciello, R., Jolivet, L., and Speranza, F., 1998, The role of pre-existing thrust faults and topography on the styles of extension in the Gran Sasso range (central Italy). Tectonophysics, 292, 229–254.

Davis, D.W., Hirdes, W., Schaltegger, U., and Nunoo, E.A., 1994, U-Pb age constraints on deposition and provenance of Birimian and gold-bearing Tarkwaian sediments in Ghana, West Africa. Precambrian Research, 67, 89–107.

Dasgupta, S. and Mukherjee, S., 2017, Brittle shear tectonics in a narrow continental rift: asymmetric non-volcanic Barmer basin (Rajasthan, India). The Journal of Geology, 125, 561–591.

De Kock, G.S., Armstrong, R.A., Siegfried, H.P., and Thomas, E., 2011, Geochronology of the Birim Supergroup of the West African craton in the Wa-Bolé region of west-central Ghana: implications for the stratigraphic framework. Journal of African Earth Sciences, 59, 1–40.

De Smet, J.H., Van Den Berg, A.P., and Vlaar, N.J., 1998, Stability and growth of continental shields in mantle convection models including recurrent melt production. Tectonophysics, 296, 15–29.

Denèle, Y., Roques, D., Ganne, J., Chardon, D., Rousse, S., and Barbey, P., 2017, Strike-slip metamorphic core complexes: gneiss domes emplaced in releasing bends. Geology, 45, 903–906.

Dioh, E., Béziat, D., Debat, P., Grégoire, M., and Ngom, P.M., 2006, Diversity of the Palaeoproterozoic granitoids of the Kédougou inlier (eastern Sénégal): petrographical and geochemical constraints. Journal of African Earth Science, 44, 351–371.

Dooley, T.P. and Schreurs, G., 2012, Analogue modelling of intraplate strike-slip tectonics: a review and new experimental results. Tectonophysics, 574, 1–71.

Ellis, S., Schreurs, G., and Panien, M., 2004, Comparisons between analogue and numerical models of thrust wedge development. Journal of Structural Geology, 26, 1659–1675.

Feng, X., 2016, Modélisation numérique des failles décrochantes et des effets de compression à grande échelle – Cas d'étude en Afrique de l'Ouest et Nouvelle Zélande. Ph.D. Thesis, Université Toulouse III-Paul Sabatier, Toulouse, 230 p.

Feng, X., Amponsah, P.O., Martin, R., Ganne, J., and Jessell, M.W., 2016a, 3-D numerical modelling of the influence of pre-existing faults and boundary conditions on the distribution of deformation: example of North-Western Ghana. Precambrian Research, 274, 161–179.

Feng, X., Wang, E., Ganne, J., Martin, R., and Jessell, M., 2018a, The exhumation along the Kenyase and Ketesso shear zones in the Sefwi terrane, West African Craton: a numerical study. Geosciences Journal. https://doi.org/10.1007/s12303-018-0057-5

Feng, X., Wang, E., Ganne, J., Amponsah, P., and Martin, R., 2018b, Role of volcano-sedimentary basins in the formation of greenstone-granitoid belts in the West African craton: a numerical model. Minerals, 8, 73. https://doi.org/10.3390/min8020073

Feng, X., Jessell, M.W., Amponsah, P.O., Martin, R., Ganne, J., Liu, D., and Batt, G., 2016b, Effect of strain-weakening on Oligocene–Miocene self-organization of the Australian-Pacific plate boundary fault in southern New Zealand: insight from numerical modelling. Journal of Geodynamics, 100, 130–143.

Farrington, R.J., Moresi, L.N., and Capitanio, F.A., 2014, The role of viscoelasticity in subducting plates. Geochemistry, Geophysics, Geosystems, 15, 4291–4304.

Feybesse, J.L., Billa, M., Guerrot, C., Duguey, E., Lescuyer, J.L., Milesi, J.P., and Bouchot, V., 2006, The paleoproterozoic Ghanaian province: geodynamic model and ore controls, including regional stress modeling. Precambrian Research, 149, 149–196.

Ganne, J. and Feng, X., 2017, Primary magmas and mantle temperatures through time. Geochemistry, Geophysics, Geosystems, 18, 872–888.

Ganne, J. and Feng, X., 2018, Magmatism: a crustal and geodynamic perspective. Journal of Structural Geology, 114, 329-335.

Ganne, J., Gerbault, M., and Block, S., 2014, Thermo-mechanical modeling of lower crust exhumation – Constraints from the metamorphic record of the Palaeoproterozoic Eburnean orogeny, West African Craton. Precambrian Research, 243, 88–109.

Ganne, J., Feng, X., Rey, P., and De Andrade, V, 2016, Statistical petrology reveals a link between supercontinents cycle and mantle global climate. American Mineralogist, 101, 2768–2773.

Ganne, J., De Andrade, V., Weinberg, R.F., Vidal, O., Dubacq, B., Kagambega, N., Naba, S., Baratoux, L., Jessell, M., and Allibon, J., 2012, Modern-style plate subduction preserved in the Palaeoproterozoic West African craton. Nature Geoscience, 5, 60–65.

Gerya, T.V. and Yuen, D.A., 2003, Rayleigh-Taylor instabilities from hydration and melting propel 'cold plumes' at subduction zones. Earth and Planetary Science Letters, 212, 47–62.

Gerya, T.V., Perchuk, L.L., and Burg, J.P., 2008, Transient hot channels: perpetrating and regurgitating ultrahigh-pressure, high-temperature crust-mantle associations in collision belts. Lithos, 103, 236–256.

Gueydan, F., Précigout, J., and Montesi, L.G., 2014, Strain weakening enables continental plate tectonics. Tectonophysics, 631, 189–196.

Hand, M. and Sandiford, M., 1999, Intraplate deformation in central Australia, the link between subsidence and fault reactivation. Tectonophysics, 305, 121–140.

Huismans, R.S. and Beaumont, C., 2002, Asymmetric lithospheric extension: the role of frictional plastic strain softening inferred from numerical experiments. Geology, 30, 211–214.

Imber, J., Tuckwell, G.W., Childs, C., Walsh, J.J., Manzocchi, T., Heath, A.E., Bonson, C.G., and Strand, J., 2004, Three-dimensional distinct element modelling of relay growth and breaching along normal faults. Journal of Structural Geology, 26, 1897–1911.

Jessell, M.W. and Lister, G.S., 1991, Strain localization behaviour in experimental shear zones. Pure and Applied Geophysics, 137, 421–438.

Jessell, M.W., Begg, G.C., and Miller, M.S., 2016, The geophysical signatures of the West African craton. Precambrian Research, 274, 3–24.

Le Pourhiet, L., Burov, E., and Moretti, I., 2004, Rifting through a stack of inhomogeneous thrusts (the dipping pie concept). Tectonics, 23. https://doi.org/10.1029/2003TC001584

Le Pourhiet, L., Huet, B., May, D.A., Labrousse, L., and Jolivet, L., 2012, Kinematic interpretation of the 3D shapes of metamorphic core complexes. Geochemistry, Geophysics, Geosystems, 13. https://doi.org/10.1029/2012GC004271

Liao, J. and Gerya, T., 2014, Influence of lithospheric mantle stratification on craton extension: insight from two-dimensional thermo-mechanical modeling. Tectonophysics, 631, 50–64.

Lister, G.S. and Davis, G.A., 1989, The origin of metamorphic core complexes and detachment faults formed during Tertiary continental extension in the northern Colorado River region, USA. Journal of Structural Geology, 11, 65–94.

Misra, A.A. and Mukherjee, S., 2015, Tectonic Inheritance in Continental Rifts and Passive Margins. Springer, Heidelberg, 88 p. https://doi.org/10.1007/978-3-319-20576-2

Moresi, L., Dufour, F., and Mühlhaus, H.B., 2003, A Lagrangian integration point finite element method for large deformation modeling of viscoelastic geomaterials. Journal of Computational Physics, 184, 476–497.

Moresi, L., Quenette, S., Lemiale, V., Meriaux, C., Appelbe, B., and Muhlhaus, H., 2007, Computational approaches to studying non-linear dynamics of the crust and mantle. Physics of the Earth and Planetary Interior, 163, 69–82.

Morley, C.K., Haranya, C., Phoosongsee, W., Pongwapee, S., Kornsawan, A., and Wonganan, N., 2004, Activation of rift oblique and rift parallel pre-existing fabrics during extension and their effect on deformation style: examples from the rifts of Thailand. Journal of Structural Geology, 26, 1803–1829.

Mulchrone, K.F. and Mukherjee, S., 2015, Shear senses and viscous dissipation of layered ductile simple shear zones. Pure and Applied Geophysics, 172, 2635–2642.

Mukherjee, S., 2011, Estimating the viscosity of rock bodies – A comparison between the Hormuz- and the Namakdan Salt Domes in the Persian Gulf, and the Tso Morari Gneiss Dome in the Himalaya. The Journal of Indian Geophysical Union, 15, 161–170.

Mukherjee, S., 2012, Simple shear is not so simple! Kinematics and shear senses in Newtonian viscous simple shear zones. Geological Magazine, 149, 819–826.

Mukherjee, S., 2013, Channel flow extrusion model to constrain dynamic viscosity and Prandtl number of the Higher Himalayan Shear Zone. International Journal of Earth Sciences, 102, 1811–1835.

Mukherjee, S., 2017, Airy's isostatic model: a proposal for a realistic case. Arabian Journal of Geosciences, 10, 268. https://doi.org/10.1007/s12517-017-3050-9

Mukherjee, S., 2018a, Moment of inertia for rock blocks subject to bookshelf faulting with geologically plausible density distributions. Journal of Earth System Science, 127, 80. https://doi.org/10.1007/s12040-018-0978-4

Mukherjee, S., 2018b, Locating center of gravity in geological contexts. International Journal of Earth Sciences, 107, 1935–1939.

Mukherjee, S. and Mulchrone, K., 2012, Estimating the viscosity and Prandtl number of the Tso Morari Gneiss Dome, western Indian Himalaya. International Journal of Earth Sciences, 101, 1929–1947.

Mukherjee, S. and Mulchrone K.F., 2013, Viscous dissipation pattern in incompressible Newtonian simple shear zones: an analytical model. International Journal of Earth Sciences, 102, 1165–1170.

Mukherjee, S. and Khonsari, M.M., 2017, Brittle rotational faults and the associated shear heating. Marine and Petroleum Geology, 88,

551–554.
Mukherjee, S. and Agarwal, I., 2018, Shear heat model for gouge free dip-slip listric normal faults. Marine and Petroleum Geology, 98, 397–400.
Mukherjee, S. and Khonsari, M.M., 2018, Inter-book normal fault-related shear heating in brittle bookshelf faults. Marine and Petroleum Geology, 97, 45–48.
Mukherjee, S., Misra, A.A., Calvès, G., and Nemčok, M., 2017, Tectonics of the Deccan Large Igneous Province: an introduction. In: Mukherjee, S., Misra, A.A., Calvès, G., and Nemčok, M. (eds.), Tectonics of the Deccan Large Igneous Province. Geological Society, London, Special Publications, 445, p. 1–9.
Neves, S.P., Vauchez, A., and Archanjo, C.J., 1996, Shear zone-controlled magma emplacement or magma-assisted nucleation of shear zones? Insights from northeast Brazil. Tectonophysics, 262, 349–364.
Neves, S.P., Vauchez, A., and Feraud, G., 2000, Tectono-thermal evolution, magma emplacement, and shear zone development in the Caruaru area (Borborema Province, NE Brazil). Precambrian Research, 99, 1–32.
O'Neill, C., Lenardic, A., Weller, M., Moresi, L., Quenette, S., and Zhang, S., 2016, A window for plate tectonics in terrestrial planet evolution? Physics of the Earth and Planetary Interiors, 255, 80–92.
Passchier, C.W. and Platt, J.P., 2017, Shear zone junctions: of zippers and freeways. Journal of Structural Geology, 95, 188–202.
Peucat, J.J., Capdevila, R., Drareni, A., Mahdjoub, Y., and Kahoui, M., 2005, The Eglab massif in the West African Craton (Algeria), an original segment of the Eburnean orogenic belt: petrology, geochemistry and geochronology. Precambrian Research, 136, 309–352.
Pinkerton, H. and Stevenson, R.J., 1992, Methods of determining the rheological properties of magmas at sub-liquidus temperatures. Journal of Volcanology and Geothermal Research, 53, 47–66.
Platt, J.P. and Passchier, C.W., 2016, Zipper junctions: a new approach to the intersections of conjugate strike-slip faults. Geology, 44, 795–798.
Ranalli, G., 1995, Rheology of the Earth. Springer, Heidelberg, 413 p.
Rey, P.F., Teyssier, C., and Whitney, D.L, 2009, The role of partial melting and extensional strain rates in the development of metamorphic core complexes. Tectonophysics, 477, 135–144.
Rey, P.F., Mondy, L., Duclaux, G., Teyssier, C., Whitney, D.L., Bocher, M., and Prigent, C., 2017, The origin of contractional structures in extensional gneiss domes. Geology, 45, 263–266.
Sharples, W., Moresi, L.N., Jadamec, M.A., and Revote, J., 2015, Styles of rifting and fault spacing in numerical models of crustal extension. Journal of Geophysical Research: Solid Earth, 120, 4379–4404.
So, B.D. and Yuen, D.A., 2014, Stationary points in activation energy for heat dissipated with a power law temperature-dependent visco-elastoplastic rheology. Geophysical Research Letters, 41, 4953–4960.
So, B.D., Yuen, D.A., Regenauer-Lieb, K., and Lee, S.M., 2012, Asymmetric lithospheric instability facilitated by shear modulus contrast: implications for shear zones. Geophysical Journal International, 190, 23–36.
Sokoutis, D., Corti, G., Bonini, M., Pierre Brun, J., Cloetingh, S., Mauduit, T., and Manetti, P., 2007, Modelling the extension of heterogeneous hot lithosphere. Tectonophysics, 444, 63–79.
Thatcher, W. and Hill, D.P., 1991, Fault orientations in extensional and conjugate strike-slip environments and their implications. Geology, 19, 1116–1120.
Tirel, C., Brun, J.P., and Sokoutis, D., 2006, Extension of thickened and hot lithospheres: inferences from laboratory modeling. Tectonics, 25. https://doi.org/10.1029/2005TC001804
Tirel, C., Brun, J.P., and Burov, E., 2008, Dynamics and structural development of metamorphic core complexes. Journal of Geophysical Research: Solid Earth, 113. https://doi.org/10.1029/2005JB003694
Vidal, M., Gumiaux, C., Cagnard, F., Pouclet, A., Ouattara, G., and Pichon, M., 2009, Evolution of a Paleoproterozoic "weak type" orogeny in the West African Craton (Ivory Coast). Tectonophysics, 477, 145–159.
Vigneresse, J.L. and Tikoff, B., 1999, Strain partitioning during partial melting and crystallizing felsic magmas. Tectonophysics, 312, 117–132.
Wang, K., Burov, E., Gumiaux, C., Chen, Y., Lu, G., Mezri, L., and Zhao, L., 2015, Formation of metamorphic core complexes in non-over-thickened continental crust: a case study of Liaodong Peninsula (East Asia). Lithos, 238, 86–100.
Weinberg, R.F., Mark, G., and Reichardt, H., 2009, Magma ponding in the Karakoram shear zone, Ladakh, NW India. Geological Society of America Bulletin, 121, 278–285.
West, M.W., 1993, Extensional reactivation of thrust faults accompanied by coseismic surface rupture, southwestern Wyoming and north-central Utah. Geological Society of America Bulletin, 105, 1137–1150.
Willingshofer, E., Sokoutis, D., and Burg, J.P., 2005, Lithospheric-scale analogue modelling of collision zones with a pre-existing weak zone. In: Gapais, D., Brun, J.P., and Cobbold, P.R. (eds.), Deformation Mechanisms, Rheology and Tectonics: from Minerals to the Lithosphere. Geological Society, London, Special Publications, 243, p. 277–294.




https://doi.org/10.1007/s12303-019-0005-z